

Size effect and atomistic deformation mechanisms of hierarchically nanotwinned fcc metals under nanoindentation

Fuping Yuan¹ · Xiaolei Wu¹

Received: 12 June 2015 / Accepted: 28 July 2015 / Published online: 5 August 2015
© Springer Science+Business Media New York 2015

Abstract Molecular dynamics simulations have been performed to investigate the atomistic deformation mechanisms of hierarchically nanotwinned Cu under nanoindentation. When the grain size (d) and the spacing of primary twins (λ_1) are fixed, the hardness is observed to increase with decreasing spacing of secondary twins (λ_2) until a critical λ_2 , and then decrease with further decreasing λ_2 . The size effect of λ_2 on the plastic area beneath the indenter is observed to be exactly opposite to the trend of the size effect on the hardness. There exist two plastic zones beneath the indenter: the severe plastic zone and the moderate plastic zone. In the severe plastic zone, high density of dislocation networks are observed and the deformation mechanisms are independent of λ_2 . The deformation mechanisms in the moderate plastic zone are highly dependent on the λ_2 , which is the origin of the size effect on the hardness. Below the critical λ_2 , the deformation mechanisms are dominated by the softening mechanisms with decreasing λ_2 : (i) detwinning of secondary twins and (ii) nucleation and propagation of partial dislocations with a small angle to the boundaries of secondary twins. Above the critical λ_2 , the deformation mechanisms are dominated by the strengthening mechanisms with decreasing λ_2 : partial dislocations are blocked by the boundaries of primary twins or secondary twins.

Introduction

Materials with improved surface contact damage resistance are always desired in the modern industry [1, 2]. Such expectations have been realized in the last several decades by tailored gradation in composition, microstructure, and the corresponding elastic/plastic properties at the material surface [3–5]. The gradient structure could be generated by the surface nanocrystallization method, such as surface mechanical attrition treatment (SMAT) [6, 7] and surface mechanical grinding treatment (SMGT) [8], in which grain size at the surface is on the order of tens of nanometer and high strength/hardness could be achieved at the surface. These developed severe plastic deformation (SPD) methods [6–8] are generally under the conditions of high strain rate and/or low temperatures, thus the hierarchically nanotwins (HNTs) could also be created at the surface in the metals and alloys especially with low or medium stacking fault energies (SFEs), such as twinning-induced plasticity (TWIP) steels [9], 304 stainless steels [10], Cu and Ni [10, 11]. These HNTs not only inherit the advantage of monolithic nanotwins [12–17], but also assemble simple nanotwins to form a new complex twinning structure for achieving higher strength/hardness and toughness [9, 11, 18–20].

The coherent twin boundaries (TBs) at the nanoscale in the single twins have been regarded as an effective way to achieve both high strength and substantial ductility [12–16]. The maximum strength is found at a critical twin boundary spacing (TBS) in the nanotwinned (NT) copper due to a transition in the dominant deformation mechanisms at the critical TBS [13, 14]. As indicated by the theoretical work based on the dislocation model and the molecular dynamics simulation work [21–25], the HNTs are much more effective for strengthening under tension than single twins and can

✉ Fuping Yuan
fpyuan@lnm.imech.ac.cn
Xiaolei Wu
xlwu@imech.ac.cn

¹ State Key Laboratory of Nonlinear Mechanics, Institute of Mechanics, Chinese Academy of Science, No.15, North 4th Ring, West Road, Beijing 100190, People's Republic of China

also reach a maximum strength by optimizing the spacing of the primary twins, the spacing of the secondary twins, and the grain size in each order (three order system). Different from those under indentation at large scale and uniform tensile deformation [26–29], our previous work [30] showed a distinct grain size effect on the hardness under nanoindentation for nanocrystalline metals, in which only inverse Hall–Petch effect was observed with the grain size up to 40 nm. For the applications of HNTs in the areas for nanocontacts, nano-tribology, and nano-machining, it is necessary to find out the size effect of TBS on the hardness and the corresponding atomistic deformation mechanisms under nanoindentation for HNTs. Is it similar or different to the grain size effect on the hardness under nanoindentation for nanocrystalline metals?

Molecular dynamics (MD) simulations have been shown to be particularly helpful for investigating the atomistic deformation mechanisms of carefully designed model structure under nanoindentation [31–34], in which the real-time responses and the stress/strain contours at the atomic level and the overall plastic area beneath the indenter could be examined. In this regard, using Cu as a model material, the size effect on the hardness and the atomistic deformation mechanisms of hierarchically NT fcc metals under nanoindentation have been investigated through a series of large-scale MD simulations in the present study.

Simulation techniques

The Large-scale Atomic/Molecular Massively Parallel Simulator (LAMMPS) code is used for MD simulations and the Ni EAM potential developed by Mishin et al. [35] is adopted for force interactions between atoms. Similar to the configuration used by Yamakov [36], all samples contain regular hexagonally shaped columnar grains with identical size in order to explore deformation mechanisms of HNTs within grains larger than those possible in fully 3-dimensional simulations. The columnar axis (z direction) is along $[\bar{1}10]$ and contains 12 atomic planes. The typical configuration for nanoindentation on the nanostructure with HNTs is shown Fig. 1a, and the atoms are colored by common neighbor analysis (CNA) values in all figures for microstructure detection. Gray color is for perfect fcc atoms, blue color is for hcp atoms, while red color stands for grain boundaries (GBs), dislocation core, free surface, and other atoms. The simulation cell contains ten grains ($d = 60$ nm) constructed by Voronoi method, and HNTs are generated within these grains. These grains are rotated with respect to each other about the columnar axis by an angle marked in each grain, and the grain orientations chosen in the present study are 0° , 30° , 45° , 60° , 90° for

simplicity, respectively. The simulation cell has the dimension sizes of $300 \times 120 \times 1.66$ nm³ and contains approximately 4,670,000 atoms. Within each grain, the primary twins are generated first, and then the boundaries for the primary twins are split into TB_{1st} and GB_{1st} when the secondary twins are generated in the primary twins, as shown in Fig. 1b. The spacing for the primary twins is denoted as λ_1 , while the spacing for the secondary twins is denoted as λ_2 . As indicated in Fig. 1b, both TB_{1st} and TB_{2nd} are special TBs with $\Sigma 3(111)$, while GB_{1st} is a boundary with $\Sigma 27(115)$. The grain size ($d = 60$ nm) and the spacing for the primary twins ($\lambda_1 = 15.03$ nm) are fixed, and the same crystallographic orientations of all ten grains and the same Voronoi grain structure are also retained when seven samples with various λ_2 (0.63, 1.04, 2.09, 3.13, 6.26, 9.39, 15.03 nm) are simulated. In Fig. 1a, the top surface is chosen as the indentation surface, while the bottom two atomic layers are set to be fixed in y direction during indentation. Periodic boundary conditions are imposed along x and z directions.

A time step of 2 fs and an velocity Verlet algorithm are used during the simulations. By the conjugate gradient method, the as-created samples are first subjected to energy minimization before indentation, and then heated up to the desired temperature (10 K) and finally relaxed under the zero pressure along x and z directions for 100 ps. This relaxation allows the whole system to release the internal stress created by the initial structure. However, during the indentation, the pressures along x and z directions are no longer zero due to the force applied by the indenter and the periodic boundary conditions along x and z directions. Thus, canonical ensemble (NVT) is used to maintain the constant volume and the constant temperature for the system during the indentation. During the indentation, the whole system is also kept at a temperature of 10 K via an external Nose–Hoover thermostat to reduce thermal fluctuations of the deformation behaviors. Of course, the mechanical response under 10 K would be different from that under room temperature since some thermally activated processes would be suppressed under cryogenic temperature. However, by keeping the same deformation temperature, the size effects of the nanostructured metals can be examined under cryogenic temperature like previous research [22, 28, 30]. Indentation is conducted in displacement control by positioning a cylindrical indenter (initially contacting with the top surface) at a constant downward speed of 50 m/s (which is much slower when compared to the wave speed), and the virtual indenter is simulated by a repulsive potential as Eq. 1:

$$F(r) = \begin{cases} -A(r - D/2)^2 & \text{for } r \leq D/2 \\ 0 & \text{for } r > D/2 \end{cases} \quad (1)$$

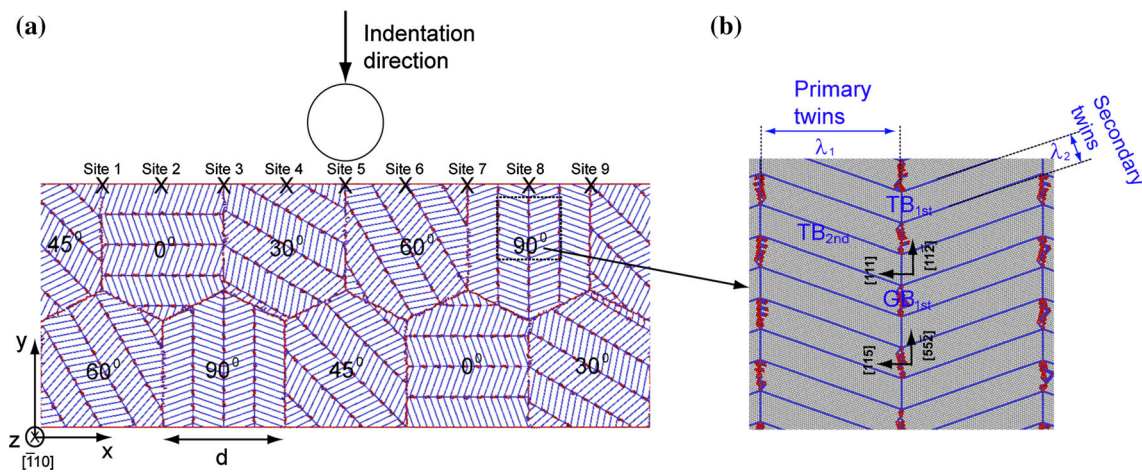


Fig. 1 (color online) **a** The configuration of nanoindentation process into the hierarchically nanotwinned Cu: $d = 60$ nm, $\lambda_1 = 15.03$ nm, $\lambda_2 = 3.13$ nm (perfect fcc atoms are not shown for clarity in this

figure). **b** The corresponding enlarged configurations showing the details for the primary twins and the secondary twins

where A ($1000 \text{ eV}/\text{\AA}^2$) is the specified force constant, r is the distance from the atom to the center of the indenter, and D (40 nm, which is much larger than the sizes of the primary twins and the second twins) is the diameter of the indenter.

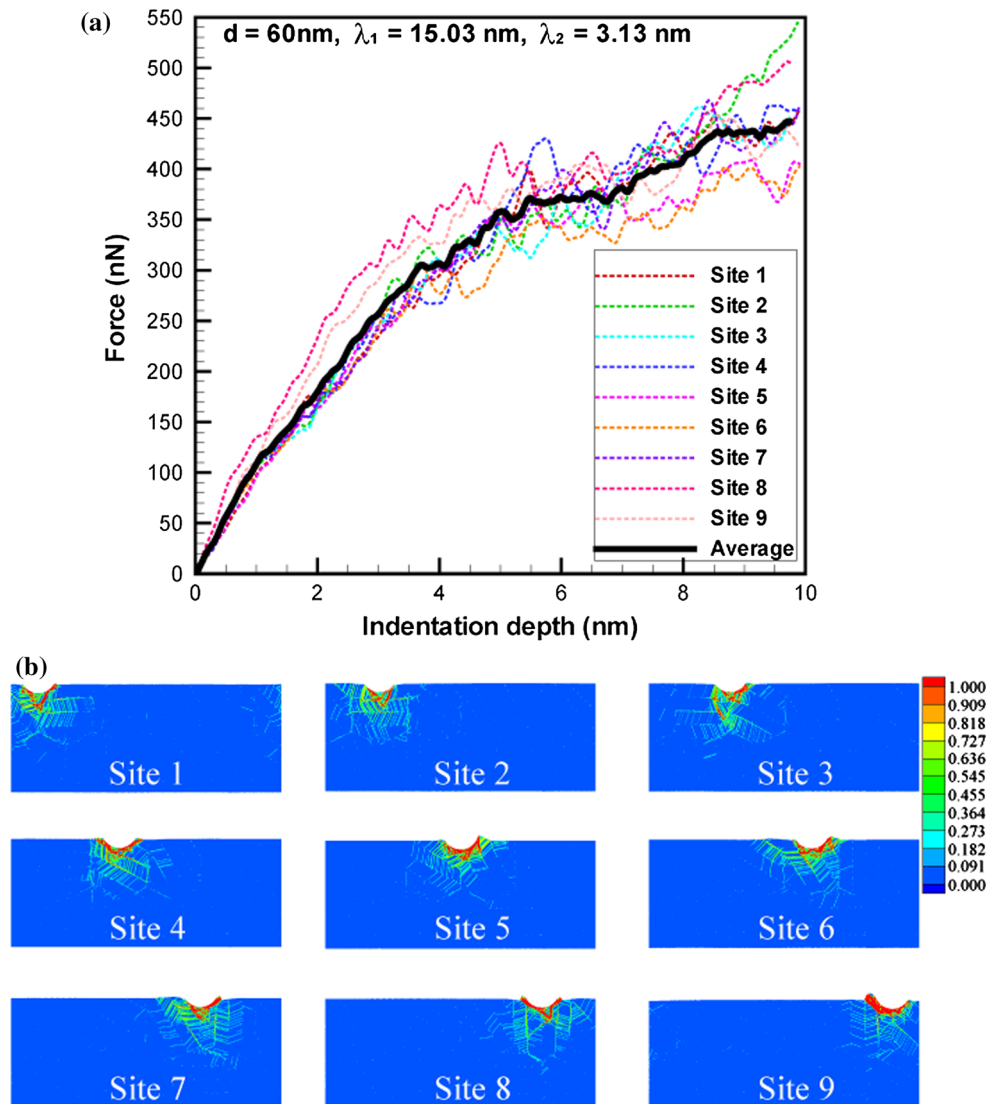
Results and discussion

For each λ_2 , nine sites are chosen evenly distributed above five grains along the top surface, as shown in Fig. 1a. One indentation test is performed at each site and the results are averaged on nine tests to mimic the sparse distributions of crystal orientation and the Schmid factors in realistic metals and alloys. So in the present work, 63 simulations in total have been performed. Figure 2a shows the force as a function of indentation depth at nine different sites for the hierarchically NT Cu with $\lambda_2 = 3.13$ nm, and the average force is obtained based on these nine indentation curves. As shown in Fig. 2a, different sites show different indentation curves, and the grain orientations beneath the indenter have strong influences on the force-depth curves. While as indicated earlier, the same crystallographic orientations of each grain (ten grains in total) and the same Voronoi grain structure are retained when λ_2 is varied, and the force for each λ_2 is averaged based on nine indentation curves, thus the orientation effects should be excluded and the average force in Fig. 2a can be used to investigate solely the size effects of λ_2 on the hardness under nanoindentation for HNTs. It also should be noted that there is negligible influence of the fixed bottom boundary on the measured force, since the maximum indentation depths are less than 10 % of the sample’s height in the y direction.

In order to obtain the detailed local strain distributions and the strain partitioning beneath the indenter, a local equivalent strain is calculated based on the atomic local strain tensor: $\varepsilon_{eq} = \sqrt{3J_2(\varepsilon)}$, where $J_2(\varepsilon)$ is the second deviatoric strain invariant. Once the reference state before the indentation is known, the current state after indentation is compared to the reference state and the local strain tensor is calculated using the all local neighbor atom’s information as a best fit of the local affine transformation [30, 37]. These local equivalent strain contours and mappings are very helpful in MD simulations, allowing us to not only obtain the plastic area beneath the indenter but also visualize microstructure, such as GBs, stacking faults (SFs), dislocations and voids, using color-encoding strain fields [30, 37]. Figure 2b shows the equivalent strain (ε_{eq}) distributions for the hierarchically NT Cu ($\lambda_2 = 3.13$ nm) indented at nine different sites. The scale bar for the contours is on the right side. It should be noted that the plastic responses at nine sites are different from each other and the grain orientations beneath the indenter have strong influence on the plastic response. So the results should also be averaged based on nine contours to minimize the grain orientation effect when the plastic area beneath the indenter is calculated for each λ_2 .

The average force curves (based on nine sites) as a function of indentation depth for the hierarchically NT Cu with various λ_2 are shown in Fig. 3a. As clearly shown in Fig. 3a, the forces increase with increasing indentation depth. In indentation process, the hardness is defined with regard to plastic deformation, and can be calculated as a ratio of the applied force to the contact area. This calculation is sometimes used while the indenter is still in contact with the applied surface (thus the area includes

Fig. 2 (color online) **a** Force as a function of indentation depth for the hierarchically nanotwinned Cu with $\lambda_2 = 3.13$ nm. **b** Equivalent strain (ϵ_{eq}) distributions for the hierarchically nanotwinned Cu ($\lambda_2 = 3.13$ nm) indented at nine different sites



both elastic and plastic deformation), and while other times is used once the indenter is removed (residual area of indentation). The former method has been used in the present study. At the early stage of indentation, the material should be still under elastic deformation, so the average hardness is calculated based on the average force curves from Fig. 3a after indentation depth of 4 nm. And the average hardness curves as a function of indentation depth for the hierarchically NT Cu with various λ_2 are shown in Fig. 3b. Then the hardness at indentation depths between 5 and 9 nm is averaged to characterize the size effect of the TBS for the secondary twins (λ_2), and the curve for this size effect is shown in Fig. 3c, where the error bars represent standard variation from indentation depth between 5 and 9 nm. The hardness increases from approximately 7.6 to 8.4 GPa as λ_2 decreases from 15.03 to 3.13 nm, and then decreases to about 7.1 GPa when λ_2 is further reduced to 0.63 nm. When the grain size (d) and the spacing of

primary twins (λ_1) are fixed, the average hardness of hierarchically NT Cu is observed to increase with decreasing λ_2 , reaching a maximum value at a critical λ_2 (about 3.13 nm), and then decrease with further decreasing λ_2 . This trend for the size effect of λ_2 on the hardness of HNTs under nanoindentation is different from the grain size effect on the hardness of nanocrystalline metals under nanoindentation [30] and is similar to the size effect of λ_2 on the strength of HNTs under uniform tensile loading [22]. This trend is also similar to the size effect of TBS on the strength of the metals with a single level of twins under uniform tensile loading [13, 14, 16], indentation [33], and shock loading [38]. The results indicate that the plastic response of the coherent TBs of the secondary twins is different from that of the general GBs under nanoindentation, and is similar to that of TBs of single twins under various loading conditions. Compared to general GBs, TBs could also provide adequate barriers and resistance to

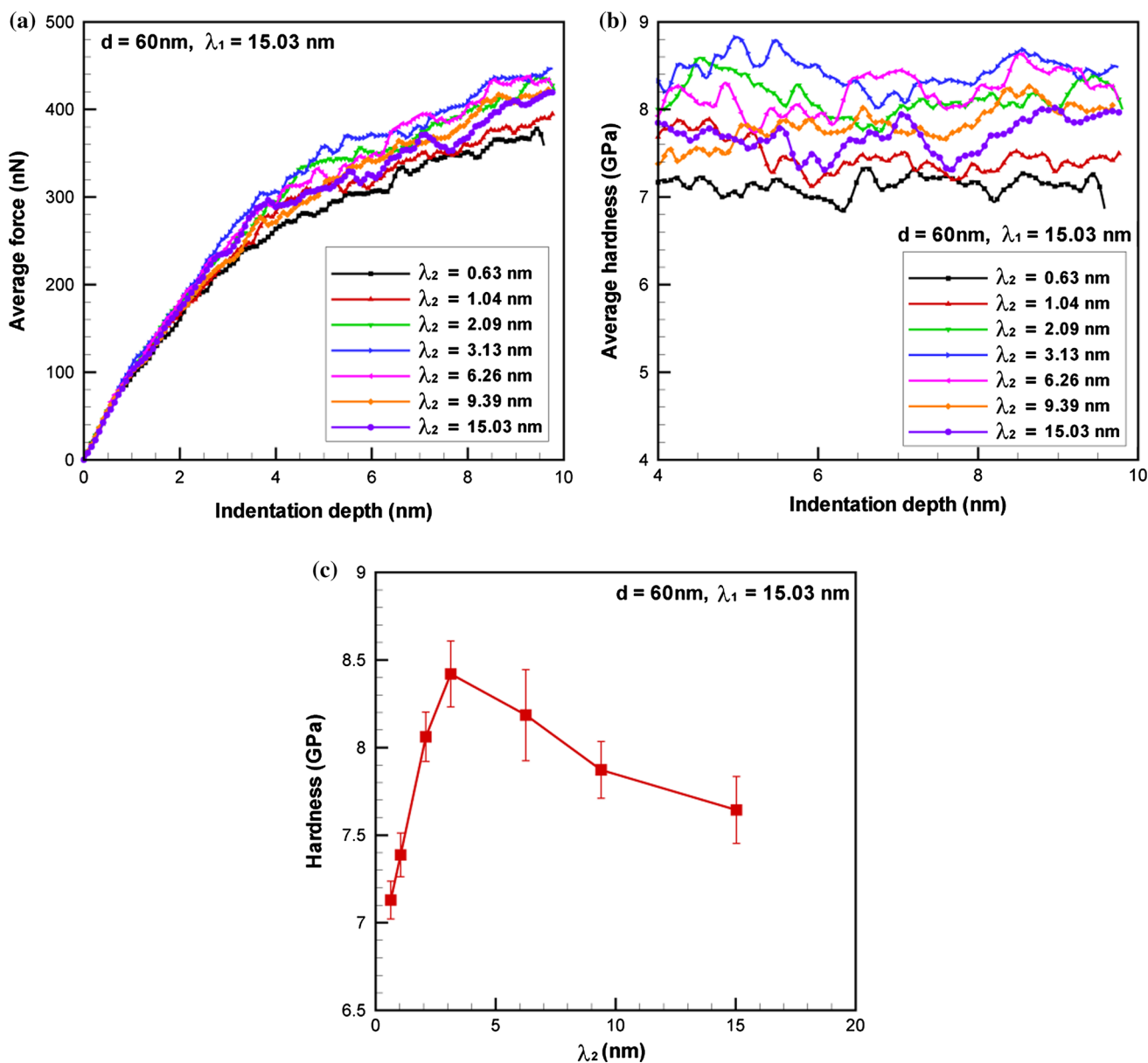


Fig. 3 (color online) **a** Average force as a function of indentation depth for the hierarchically nanotwinned Cu with various λ_2 . **b** Average hardness as a function of indentation depth for the

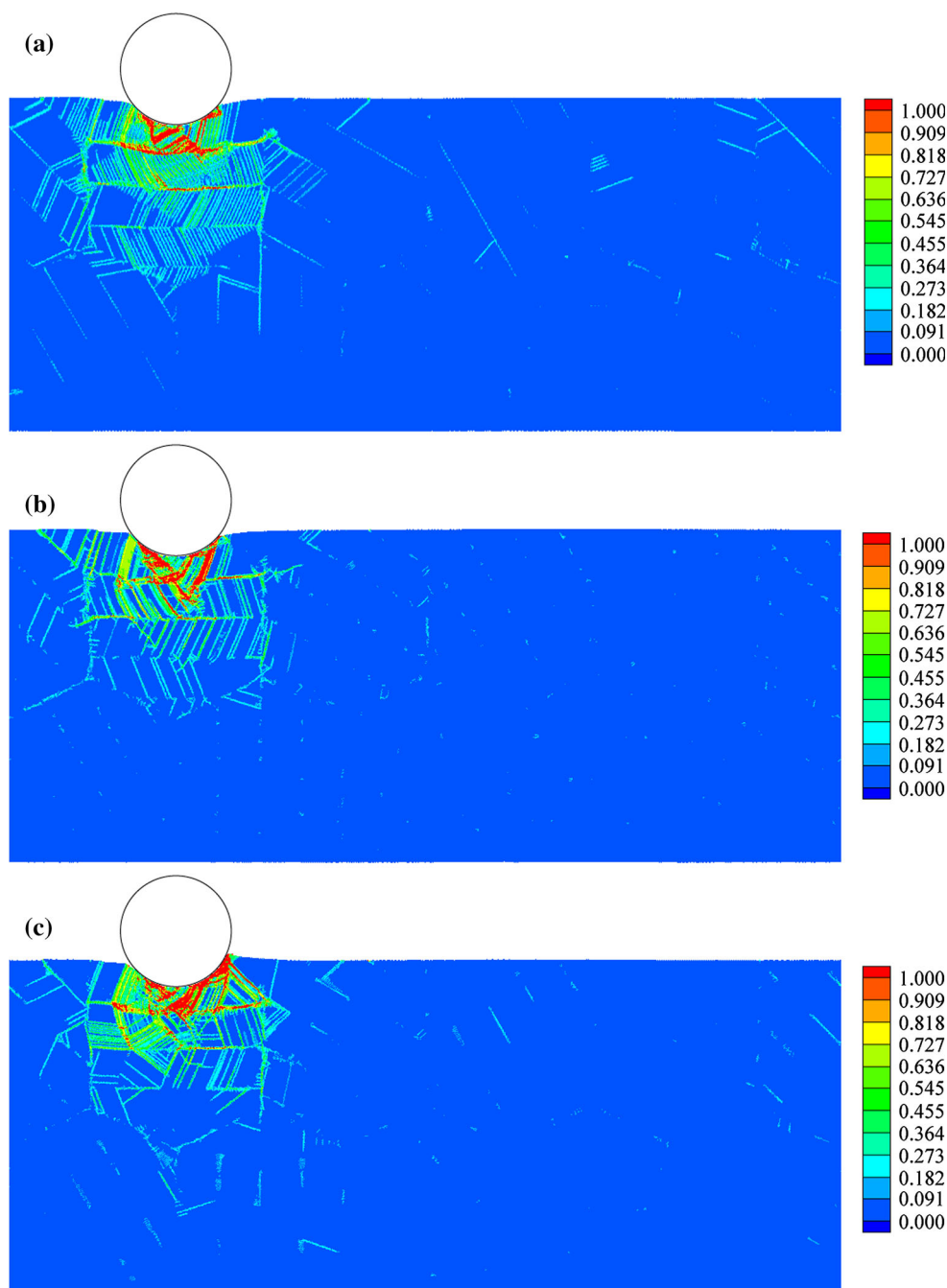
hierarchically nanotwinned Cu with various λ_2 . **c** Hardness versus spacing for the secondary twins (λ_2)

dislocation motion for strengthening under nanoindentation when TBS is large [33] since they possess lower excess energies and exhibit much higher thermal and mechanical stability. The trend shown in Fig. 3c will also be discussed later based on the plastic area and the detailed atomistic deformation mechanisms beneath the indenter.

Figure 4 shows the equivalent strain (ϵ_{eq}) distributions indented at site 2 for the hierarchically NT Cu with three typical λ_2 (0.63, 3.13, and 15.03 nm). The scale bars for the contours are on the right side of the figure. Based on these strain contours, the detailed observations could be

summarized as follows: (i) large local strains are accumulated and observed at areas of SFs, the general GBs and the boundaries of the primary twins and the secondary twins; (ii) the largest strain zone is observed to accumulate at the areas adjacent to the indenter, and the magnitude of the strain gradually decreases with increasing distance from the indenter; (iii) at the areas close to the indenter, two of slip planes are activated in the section of primary twins independent of λ_2 , which allows the emission and the propagation of partial dislocations, leaving SFs behind; (iv) at the areas a little far away from the indenter, only one slip

Fig. 4 (color online) Equivalent strain (ε_{eq}) distributions indented at site 2 for the hierarchically nanotwinned Cu with various λ_2 : **a** $\lambda_2 = 0.63$ nm **b** $\lambda_2 = 3.13$ nm **c** $\lambda_2 = 15.03$ nm



plane is activated in the section of primary twins for the case of small λ_2 , while two slip planes are still activated when λ_2 is large.

As we know, hardness is a measure of the materials for resisting plastic deformation, and less plastic area under indentation should be generated for the materials with higher hardness. Figure 5 shows the plastic zones beneath the indenter for the hierarchically NT Cu at two typical sites (sites 1 and 6) with three typical λ_2 (0.63, 3.13, and 15.03 nm). The plastic zones shown in red are determined by regions where $\varepsilon_{eq} > 0.2$, while the green color

represents regions with smaller strain ($\varepsilon_{eq} \leq 0.2$). The area of the plastic zone is calculated based on these red areas. At site 1, the plastic area for $\lambda_2 = 0.63$ nm is 1917 nm², the plastic area for $\lambda_2 = 3.13$ nm is 1386 nm², while the plastic area for $\lambda_2 = 15.03$ nm is 1433 nm². It is noted that the lowest plastic area is always observed for $\lambda_2 = 3.13$ nm at each site, indicating the highest hardness, which agrees well with the results in Fig. 3c.

The area of plastic zone beneath the indenter should also be averaged based on nine different sites to exclude the grain orientation effect and show the size effect of λ_2

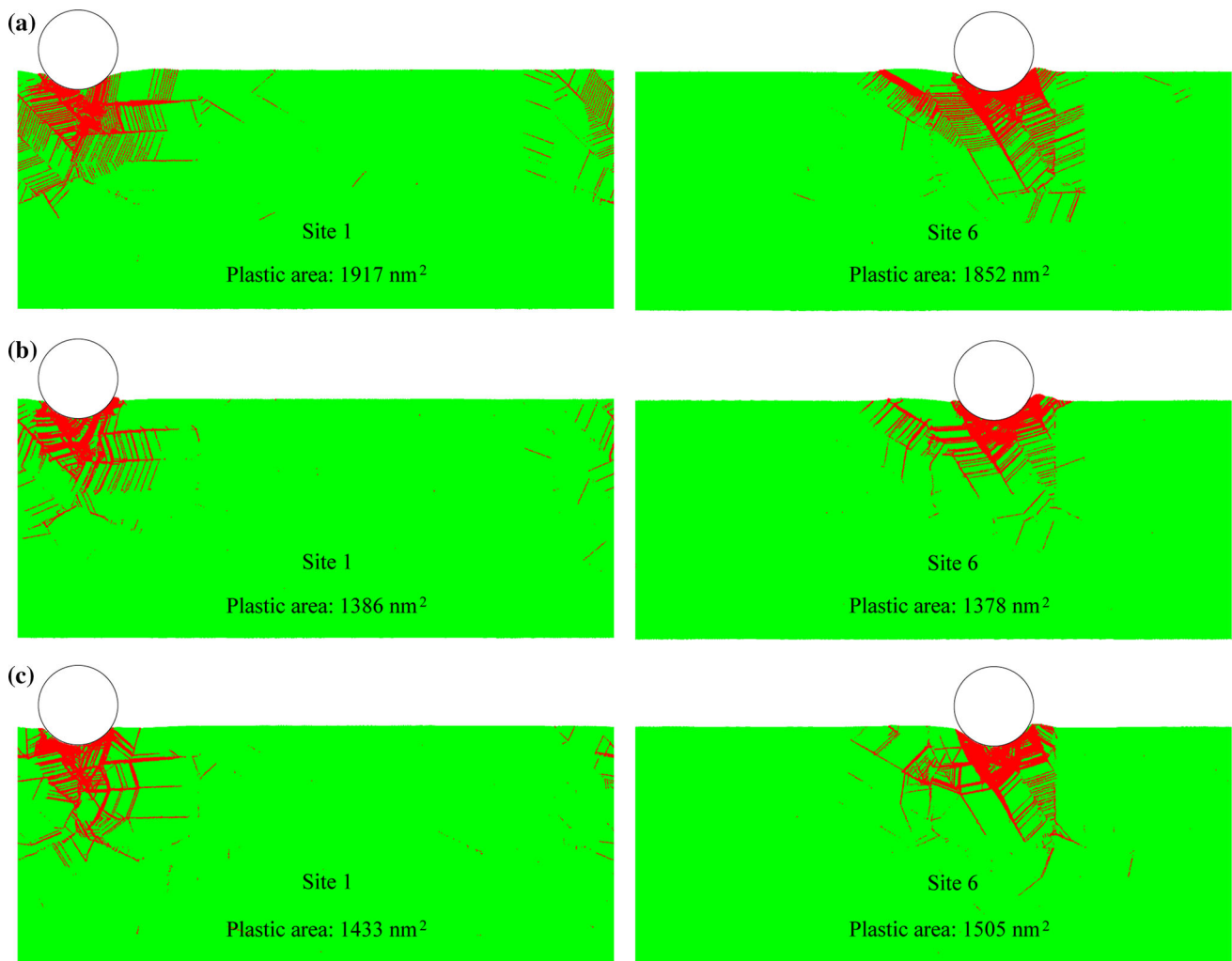


Fig. 5 (color online) Plastic zones beneath the indenter for the hierarchically nanotwinned Cu with various λ_2 (red color is for regions with $\varepsilon_{\text{eq}} > 0.2$, while the green color represents the regions with $\varepsilon_{\text{eq}} \leq 0.2$): **a** $\lambda_2 = 0.63$ nm **b** $\lambda_2 = 3.13$ nm **c** $\lambda_2 = 15.03$ nm

only. In this regard, the average plastic areas beneath the indenter based on nine sites as a function of λ_2 are shown in Fig. 6. The error bars represent standard variation from indentations performed at nine different sites. The area of plastic zone beneath the indenter is observed to be strongly dependent on λ_2 , and the size effect of the secondary twins on the plastic area is observed to decrease with increasing λ_2 first, reaching a minimum value at a critical λ_2 , and then increase as λ_2 is further reduced. This trend for λ_2 on the plastic area is exactly opposite to the trend for λ_2 on the hardness, as shown in Fig. 3c, and the critical λ_2 for the plastic area also coincides with that for the hardness.

Atomic level analysis of the deformed configurations is conducted in order to understand the deformation mechanisms for hierarchically NT Cu under nanoindentation. Figure 7 shows the simulated deformation patterns (at site 2) at indentation depth of 9.5 nm for the hierarchically NT

Cu with three typical λ_2 (0.63, 3.13, and 15.03 nm). Perfect fcc atoms are not shown in the left figures for the clarity, and the corresponding enlarged configurations for the marked rectangular areas are shown in the right figures. Two different plastic zones beneath the indenter are observed: the severe plastic zone adjacent to the indenter and the moderate plastic zone away from the indenter. In the severe plastic zone, high density of dislocations and dislocation networks by dislocation interactions are observed, and the atomistic deformation mechanisms are independent of λ_2 . In the area adjacent to the indenter, high hydrostatic pressure and very complex stress state exist, thus deformation compatibility at various boundaries ($\text{GB}_{1\text{st}}$, $\text{TB}_{1\text{st}}$, and $\text{TB}_{2\text{nd}}$) usually requires the simultaneous operations of several slip systems, which possibly forces these boundaries to be potential nucleating sites for numerous dislocations and the subsequent formation of dislocation networks.

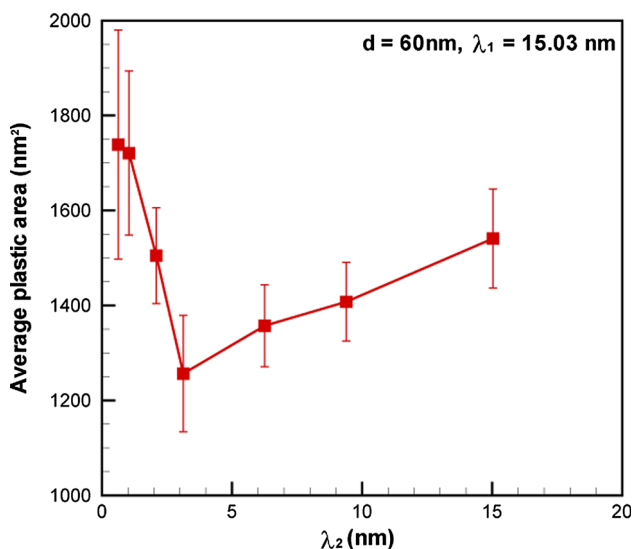


Fig. 6 (color online) The average area of plastic zone beneath the indenter as a function of spacing for the secondary twins (λ_2)

However, the atomistic deformation mechanisms in the moderate plastic zone are highly dependent on the λ_2 , which could be the origin of the size effect on the hardness. Figure 8 shows the enlarged simulated deformation

patterns at indentation depth of 9.5 nm for the hierarchically NT Cu with $\lambda_2 = 0.63$ and 15.03 nm showing the two softening mechanisms for small λ_2 and the two strengthening mechanisms for large λ_2 . As shown in Fig. 8a, b, below the critical λ_2 , the deformation mechanisms in the moderate plastic zone are dominated by the following two softening mechanisms with decreasing λ_2 : (i) detwinning of the secondary twins; and (ii) nucleation and propagation of partial dislocations with a small angle to the twin boundary of the secondary twins. In the previous work [14], the stress required to move dislocations parallel or with a small angle to the TBs has been shown to be on the order of 10 MPa, which is negligible when compared to the strength of HNTs. Therefore, when the above two deformation mechanisms are the dominant deformation mechanism, the plastic behavior of the hierarchically NT Cu should be controlled by the nucleation rate of dislocations parallel to TB_{2nd} since dislocations could glide easily along TB_{2nd} once they are nucleated. Below the critical λ_2 , smaller λ_2 means higher density of intersection sites between TB_{2nd} and boundaries of the primary twins, resulting in larger number of nucleation sources and higher nucleation rate of dislocations parallel to TB_{2nd} , then causing the softening behaviors on the hardness of hierarchically NT Cu [14, 39].

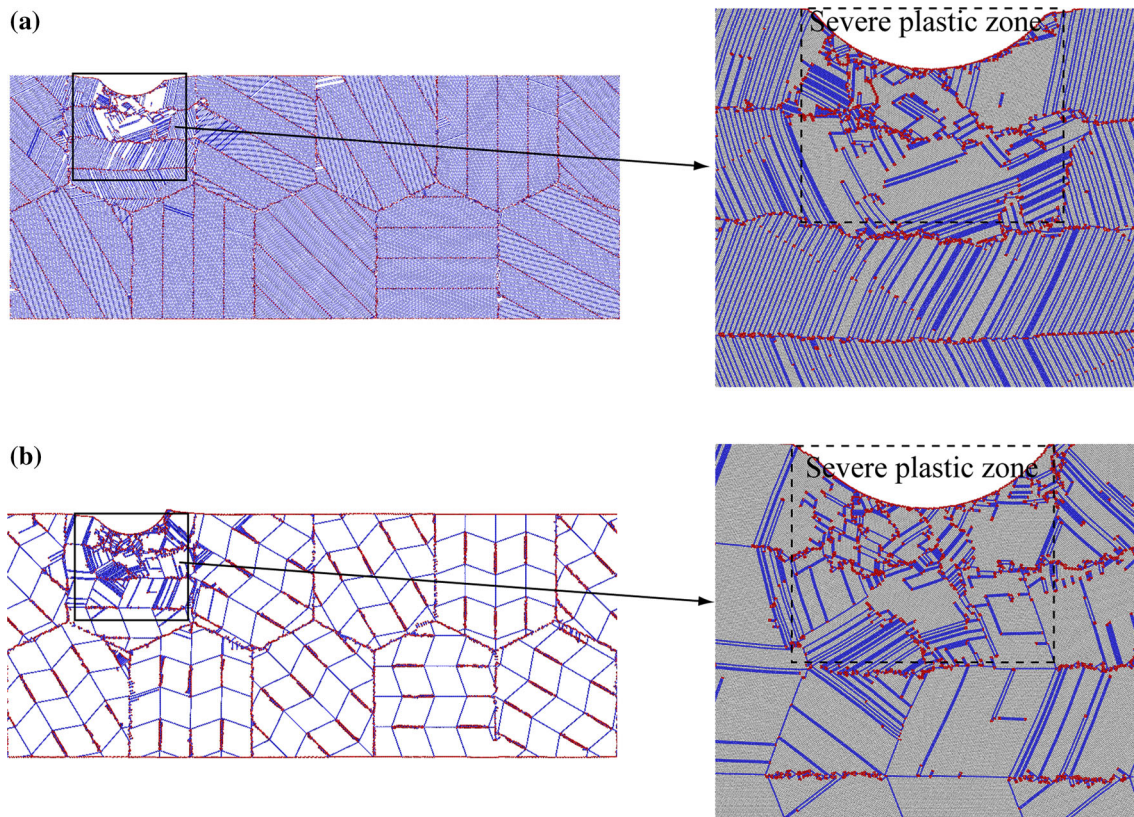


Fig. 7 (color online) Simulated deformation patterns (at site 2) at indentation depth of 9.5 nm for the hierarchically nanotwinned Cu with various λ_2 : **a** $\lambda_2 = 0.63$ nm **b** $\lambda_2 = 15.03$ nm

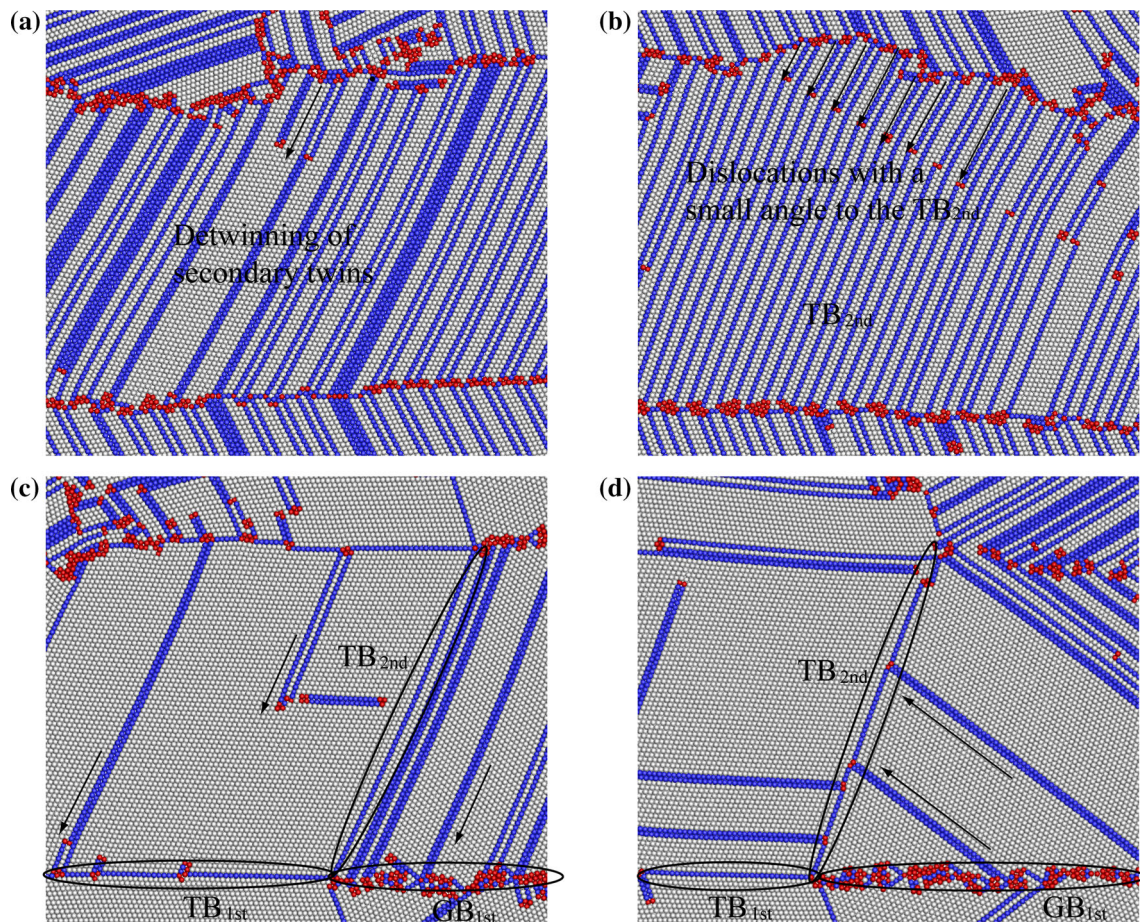


Fig. 8 (color online) **a, b** Enlarged simulated deformation patterns at indentation depth of 9.5 nm for the hierarchically nanotwinned Cu with $\lambda_2 = 0.63$ nm showing the two softening mechanisms. **c,**

d Enlarged simulated deformation patterns at indentation depth of 9.5 nm for the hierarchically nanotwinned Cu with $\lambda_2 = 15.03$ nm showing the two strengthening mechanisms

As shown in Fig. 8c, d, above the critical λ_2 , the deformation mechanisms in the moderate plastic zone are dominated by the following two strengthening mechanisms with decreasing λ_2 : (i) partial dislocations nucleated from various boundaries intersect with and are blocked by the boundaries of the primary twins (GB_{1st} and TB_{1st}); and (ii) partial dislocations nucleated from various boundaries intersect with and are blocked by the twin boundaries of the secondary twins (TB_{2nd}). As summarized in the previous research [39], four possible dislocation-TB reaction processes exist in NT metals and two of them involve the formation of immobile dislocation locks for strengthening and hardening, in which one process is very similar to our case. Previous research [32, 33] also suggested that a planar TB below the indenter (with a distance away from the indenter) and TBs in nanocrystalline metals (with large TBS) are effective obstacles to the motion of dislocations and change the dislocation patterns dominating the deformation, and could provide greater resistance to the plastic deformation than the twin-free crystal.

It should be noted that only the size effect of the secondary twins (λ_2) on the hardness and the corresponding atomistic deformation mechanisms of hierarchically NT metals have been considered. The influences of other parameters (i.e., the grain size d and the spacing of primary twins λ_1) need to be explored in the future study. Moreover, although five hexagonal grains with different orientations have been considered, the conclusions obtained from the present study are only the first step to understand the atomistic deformation behaviors of hierarchically NT metals under nanoindentation, more realistic models containing larger number of grains with different shapes and various orientations, and even the true three-dimensional models should also be explored in the future research.

Concluding remarks

In the present study, the size effect of the secondary twins (λ_2) on the hardness and the corresponding atomistic deformation mechanisms of hierarchically

NT Cu with fixed grain size (d) and fixed spacing of the primary twins (λ_1) under nanoindentation have been investigated using a series of large-scale MD simulations. The main findings are summarized as follows:

1. The average hardness of hierarchically NT Cu increases with decreasing spacing of secondary twins (λ_2), reaching a maximum value at a critical λ_2 , and then decrease with further decreasing λ_2 . Moreover, the plastic area beneath the nanoindenter is examined for the hierarchically NT Cu, the size effect of λ_2 on the plastic area is observed to be exactly opposite to the trend of size effect on the hardness, which agrees well with that less plastic area under indentation should result in higher hardness.
2. Two different plastic zones beneath the indenter are observed: the severe plastic zone adjacent to the indenter and the moderate plastic zone away from the indenter.
3. Independent of λ_2 , high density of dislocations and dislocation networks by dislocation interactions are observed in the severe plastic zone due to high hydrostatic pressure and very complex stress state existing at the area adjacent to the indenter.
4. However, the spacing of secondary twins (λ_2) has strong influence on the atomistic deformation mechanisms in the moderate plastic zone, which could be the origin of the size effect of λ_2 on the hardness. Below the critical λ_2 , the deformation mechanisms in the moderate plastic zone are dominated by the two softening mechanisms with decreasing λ_2 : (i) detwinning of the secondary twins; and (ii) nucleation and propagation of partial dislocations with a small angle to the twin boundary of the secondary twins. Above the critical λ_2 , the deformation mechanisms are dominated by the two Hall–Petch type strengthening mechanisms with decreasing λ_2 : (i) partial dislocations nucleated from various boundaries intersect with and are blocked by the boundaries of the primary twins (GB_{1st} and TB_{1st}); and (ii) partial dislocations nucleated from various boundaries intersect with and are blocked by the twin boundaries of the secondary twins (TB_{2nd}).

Acknowledgements The authors would like to thank the financial support by National Natural Science Foundation of China (Nos. 11222224, 11472286 and 11021262) and National Key Basic Research Program of China (Grants Nos. 2012CB932203 and 2012CB937500). The simulations reported in the present work were performed at Supercomputing Center of Chinese Academy of Sciences.

References

1. Suresh S (2001) Graded materials for resistance to contact deformation and damage. *Science* 292:2447–2451
2. Ke LL, Wang YS (2006) Two-dimensional contact mechanics of functionally graded materials with arbitrary spatial variations of material properties. *Int J Solids Struct* 43:5779–5798
3. Roland T, Reirant D, Lu K, Lu J (2006) Fatigue life improvement through surface nanostructuring of stainless steel by means of surface mechanical attrition treatment. *Scr Mater* 54:1949–1954
4. Shukla A, Jain N, Chona R (2007) A review of dynamic fracture studies in functionally graded materials. *Strain* 43:76–95
5. Choi IS, Detor AJ, Schwaiger R, Dao M, Schuh CA, Suresh S (2008) Mechanics of indentation of plastically graded materials-II: experiments on nanocrystalline alloys with grain size gradients. *J Mech Phys Solids* 56:172–183
6. Lu K, Lu J (2004) Nanostructured surface layer on metallic materials induced by surface mechanical attrition treatment. *Mater Sci Eng A* 375–377:38–45
7. Wang K, Tao NR, Liu G, Lu J, Lu K (2006) Plastic strain-induced grain refinement at the nanometer scale in copper. *Acta Mater* 54:5281–5291
8. Fang TH, Li WL, Tao NR, Lu K (2011) Revealing extraordinary intrinsic tensile plasticity in gradient nano-grained copper. *Science* 331:1587–1590
9. Kou HN, Lu J, Li Y (2014) High-strength and high-ductility nanostructured and amorphous metallic materials. *Adv Mater* 26:5518–5524
10. Tao NR, Lu K (2009) Nanoscale structural refinement via deformation twinning in face-centered cubic metals. *Scr Mater* 60:1039–1043
11. Zhu YT, Narayan J, Hirth JP, Mahajan S, Wu XL, Liao XZ (2009) Formation of single and multiple deformation twins in nanocrystalline fcc metals. *Acta Mater* 57:3763–3770
12. Afanasyev KA, Sansoz F (2007) Strengthening in gold nanopillars with nanoscale twins. *Nano Lett* 7:2056–2062
13. Lu L, Chen X, Huang X, Lu K (2009) Revealing the maximum strength in nanotwinned copper. *Science* 323:607–610
14. Li XY, Wei YJ, Lu L, Lu K, Gao HJ (2010) Dislocation nucleation governed softening and maximum strength in nano-twinned metals. *Nature* 464:877–880
15. Zhu LL, Ruan HH, Li XY, Dao M, Gao HJ, Lu J (2011) Modeling grain size dependent optimal twin spacing for achieving ultimate high strength and related high ductility in nanotwinned metals. *Acta Mater* 59:5544–5557
16. Zhu YT, Liao XZ, Wu XL (2012) Deformation twinning in nanocrystalline materials. *Prog Mater Sci* 57:1–62
17. Zhu YT, Liao XZ, Wu XL, Narayan J (2013) Grain size effect on deformation twinning and detwinning. *J Mater Sci* 48:4467–4475. doi:10.1007/s10853-013-7140-0
18. Müllner P, King AH (2010) Deformation of hierarchically twinned martensite. *Acta Mater* 58:5242–5261
19. Yuan FP, Wu XL (2013) Formation sequences and roles of multiple deformation twins during the plastic deformation in nanocrystalline fcc metals. *Mater Sci Eng A* 580:58–65
20. Wei YJ, Li YQ, Zhu LC, Liu Y, Lei XQ, Wang G, Wu YX, Mi ZL, Liu JB, Wang HT, Gao HJ (2014) Evading the strength-ductility trade-off dilemma in steel through gradient hierarchical nanotwins. *Nat Commun* 5:3580
21. Zhu LL, Kou HN, Lu J (2012) On the role of hierarchical twins for achieving maximum yield strength in nanotwinned metals. *Appl Phys Lett* 101:081906

22. Yuan FP, Wu XL (2013) Size effect of primary/secondary twins on the atomistic deformation mechanisms in hierarchically nanotwinned metals. *J Appl Phys* 113:203516
23. Yuan FP, Wu XL (2013) Atomistic scale fracture behaviours in hierarchically nanotwinned metals. *Philos Mag* 93:3248–3259
24. Sun LG, He XQ, Zhu LL, Lu J (2014) Two softening stages in nanotwinned Cu. *Philos Mag* 94:4037–4052
25. Zhu LL, Qu SX, Guo X, Lu J (2015) Analysis of the twin spacing and grain size effects on mechanical properties in hierarchically nanotwinned face-centered cubic metals based on a mechanism-based plasticity model. *J Mech Phys Solids* 76:162–179
26. Schiøtz J, Jacobsen KW (2003) A maximum in the strength of nanocrystalline copper. *Science* 301:1357–1359
27. Meyers MA, Mishra A, Benson DJ (2006) Mechanical properties of nanocrystalline materials. *Prog Mater Sci* 51:427–556
28. Pan ZL, Li YL, Wei Q (2008) Tensile properties of nanocrystalline tantalum from molecular dynamics simulations. *Acta Mater* 56:3470–3480
29. Jeon JB, Lee BJ, Chang YW (2011) Molecular dynamics simulation study of the effect of grain size on the deformation behavior of nanocrystalline body-centered cubic iron. *Scr Mater* 64:494–497
30. Liu XM, Yuan FP, Wei YG (2013) Grain size effect on the hardness of nanocrystal measured by the nanosize indenter. *Appl Surf Sci* 279:159–166
31. Hasnaoui A, Derlet PM, Van Swygenhoven H (2004) Interaction between dislocations and grain boundaries under an indenter—a molecular dynamics simulation. *Acta Mater* 52:2251–2258
32. Kulkarni Y, Asaro RJ, Farkas D (2009) Are nanotwinned structures in fcc metals optimal for strength, ductility and grain stability? *Scr Mater* 60:532–535
33. Qu SX, Zhou HF (2010) Hardening by twin boundary during nanoindentation in nanocrystals. *Nanotechnology* 21:335704
34. Sansoz F, Stevenson KD (2011) Relationship between hardness and dislocation processes in a nanocrystalline metal at the atomic scale. *Phys Rev B* 83:224101
35. Mishin Y, Farkas D, Mehl MJ, Papaconstantopoulos DA (1999) Interatomic potentials for monoatomic metals from experimental data and ab initio calculations. *Phys Rev B* 59:3393–3407
36. Yamakov V, Wolf D, Phillpot SR, Mukherjee AK, Gleiter H (2002) Dislocation processes in the deformation of nanocrystalline aluminium by molecular-dynamics simulation. *Nat Mater* 1:45–48
37. Shimizu F, Ogata S, Li J (2007) Theory of shear banding in metallic glasses and molecular dynamics calculations. *Mater Trans* 48:2923–2927
38. Yuan FP, Wu XL (2012) Shock response of nanotwinned copper from large-scale molecular dynamics simulations. *Phys Rev B* 86:134108
39. Lu L, You ZS, Lu K (2012) Work hardening of polycrystalline Cu with nanoscale twins. *Scr Mater* 66:837–842